VI International Conference on Computational Methods for Coupled Problems in Science and Engineering
COUPLED PROBLEMS 2015
B. Schrefler, E. Oñate and M. Papadrakakis(Eds)

EXTENSION OF THE LS-STAG IMMERSED BOUNDARY METHOD FOR RANS-BASED TURBULENCE MODELS AND ITS APPLICATION FOR NUMERICAL SIMULATION IN COUPLED HYDROELASCTIC PROBLEMS

VALERIA V. PUZIKOVA AND ILIA K. MARCHEVSKY

Bauman Moscow State Technical University (BMSTU)
Applied Mathematics department
Russia, 105005 Moscow, 2nd Baumanskaya, 5
e-mail: valeria.puzikova@gmail.com, iliamarchevsky@mail.ru

Key words: Immersed Boundary Methods, The LS-STAG Method, Coupled Hydroelastic Problems, The Spalart-Allmaras RANS Model, Multigrid Methods

Abstract. The general approach to the application of the LS-STAG method for RANS simulation and for numerical simulation in coupled hydroelastic problems is suggested. According to the concept of the LS-STAG method normal Reynolds stress components are sampled on the base mesh (similar to pressure discretization) and shear ones are sampled in the upper right corners of the base mesh cells. Thus, for the shear Reynolds stresses an additional mesh (xy-mesh) is introduced. In this research the LS-STAG-discretization for convective and diffusive fluxes on the xy-mesh is developed. A software package is developed for numerical solution of the Navier-Stokes and Reynolds-averaged Navier-Stokes equations by using the LS-STAG method. To validate this approach and developed software package the flow past circular airfoil at the Reynolds numbers Re = 1000 and Re = 3900 was simulated. Some numerical results are also presented for simulation of a circular airfoil wind resonance phenomenon.

1 INTRODUCTION

Immersed boundary methods [1] have become popular in Computational Fluid Dynamics over recent years for simulating flows through complex solid geometries and in coupled hydroelasctic problems. The advantage of these methods over a method with a body-fitted mesh is their computational efficiency: they do not require regridding when domain shape changes in the simulation process due to hydroelastic body motion.

The LS-STAG method [2] for viscous incompressible flows simulation combines the advantages of immersed boundary methods, the marker and cells (MAC) method and level-set [3] method. The LS-STAG method allows to solve on the Cartesian meshes such

complicated problems of computational mechanics as coupled hydroelastic problems. In contrast to classical immersed boundary methods, the flow variables are computed in the cut-cells, and not interpolated. Moreover, the LS-STAG discretization in the cut-cells is performed by the same formulae as in rectangular cells. Numerical analogues of total mass, momentum and kinetic energy conservation laws in each cell is a base of LS-STAG discretization constructing, which allows to obtain physically realistic numerical solution.

However, the LS-STAG method, as all mesh methods has a significant limitation when simulating flows with high Reynolds number: it requires extremely small space and time steps. It leads to significant increase in computational cost. The traditional method of solving this problem is Reynolds averaged Navier—Stokes (RANS) simulation, Large Eddy Simulation (LES), Detached Eddy Simulation (DES) *etc.* [4] usage. However, as the analysis of the literature shows such modifications of the LS-STAG method currently do not exist. Therefore the purpose of this study is the constructing of the LS-STAG method extension for the numerical solution of two-dimensional RANS equations. This modification of the LS-STAG method is presented below.

2 GOVERNING EQUATIONS

Two-dimensional RANS equations is considered:

$$\nabla \cdot \mathbf{v} = 0, \quad \frac{\partial \mathbf{v}}{\partial t} + (\mathbf{v} \cdot \nabla)\mathbf{v} = \nabla p + \frac{1}{\mathrm{Re}}\Delta \mathbf{v} + \nabla \cdot \hat{\tau}^{\,t}. \tag{1}$$

Here $\mathbf{v} = \mathbf{v}(x, y, t) = u \cdot \mathbf{e}_x + v \cdot \mathbf{e}_y$ is the dimensionless Reynolds averaged velocity, $p = p(x, y, t)$ is the dimensionless Reynolds averaged pressure, $\hat{\tau}^t$ is the Reynolds stresses tensor. The relationship between $\hat{\tau}^t$ and flow Reynolds averaged variables is given by the turbulence model.

The boundary conditions on the computational domain are the following:

$$\mathbf{v}\big|_{\text{inlet}} = \mathbf{v}_\infty, \quad \frac{\partial \mathbf{v}}{\partial \mathbf{n}}\Big|_{\text{outlet}} = 0, \quad \frac{\partial p}{\partial \mathbf{n}}\Big|_{\text{inlet\&outlet}} = 0, \tag{2}$$

and boundary conditions on the airfoil are no-slip conditions:

$$\mathbf{v}\big|_{\text{airfoil}} = \mathbf{v}^{\text{ib}}, \quad \frac{\partial p}{\partial \mathbf{n}}\Big|_{\text{airfoil}} = 0. \tag{3}$$

Here $\mathbf{v}^{\text{ib}}$ is the velocity of the immersed boundary. The airfoil assumed to be rigid and it can oscillate with 1, 2 or 3 degrees of freedom. Its motion is described by dynamics equations:

$$\ddot{\vec{q}} = \vec{\Phi}(\vec{q}, \dot{\vec{q}}) + \vec{Q}^{\text{flow}} + \vec{Q}^{\text{ext}}. \tag{4}$$

Here $\vec{q}$ is the airfoil generalized coordinates vector, $\vec{\Phi}(\vec{q}, \dot{\vec{q}})$ is determined by elastic and viscous constraints imposed on the airfoil, $\vec{Q}^{\text{flow}}$ is the generalized aerodynamic force, $\vec{Q}^{\text{ext}}$ is external mass generalized forces vector.

In case of Reynolds Stress (RSM) RANS models the Reynolds stress transport equation is solved for simulating of $\hat{\tau}^{\,t}$. In case of Eddy Viscosity (EVM) RANS models the

eddy viscosity ν^t (and the turbulent kinetic energy k in case of two-equation models) is simulated and Reynolds stresses are evaluated using the Boussinesq assumption [4]:

$$\hat{\tau}^t = \nu^t \begin{pmatrix} 2\dfrac{\partial u}{\partial x} & \dfrac{\partial u}{\partial y} + \dfrac{\partial v}{\partial x} \\ \dfrac{\partial u}{\partial y} + \dfrac{\partial v}{\partial x} & 2\dfrac{\partial v}{\partial y} \end{pmatrix} + \frac{2}{3} k \hat{I}. \tag{5}$$

Here $\hat{I}$ is the second-order unit tensor.

In this study the details of the LS-STAG discretization constructing for EVM RANS approach are presented on example of the Spallart—Allmaras (S-A) turbulence model [5]. In this model the turbulent kinetic energy is assumed to be close to zero ($k \approx 0$). Thus, the following formulae for normal (6) and shear (7) Reynolds stresses are obtained from (5):

$$\tau^t_{xx} = 2\nu^t \frac{\partial u}{\partial x}, \quad \tau^t_{yy} = 2\nu^t \frac{\partial v}{\partial y}, \tag{6}$$

$$\tau^t_{xy} = \nu^t \left(\frac{\partial u}{\partial y} + \frac{\partial v}{\partial x} \right). \tag{7}$$

The eddy viscosity in the Spallart—Allmaras turbulence model is given by the following equations:

$$\nu^t = \tilde{\nu} f_{\nu 1}, \quad \frac{\partial \tilde{\nu}}{\partial t} + (\mathbf{v} \cdot \nabla)\tilde{\nu} = P^\nu - D^\nu + \frac{1}{\sigma} \nabla \cdot [(\nu + \tilde{\nu}) \nabla \tilde{\nu}] + \frac{c_{b2}}{\sigma} (\nabla \tilde{\nu})^2. \tag{8}$$

Here $\tilde{\nu}$ is the S-A working variable, $D^\nu = \left(c_{w1} f_w - \dfrac{c_{b1}}{\varkappa^2} f_{t2} \right) \left(\dfrac{\tilde{\nu}}{d} \right)^2$ is the destruction term, $P^\nu = c_{b1}[1 - f_{t2}]\tilde{S}$ is the production term, d is the dimensionless distance from the field point to the nearest wall, ν is the dimensionless viscosity, $f_{t2} = c_{t3} \cdot e^{-c_{t4}\chi^2}$, $g = r + c_{w2}(r^6 - r)$, $c_{w1} = \dfrac{c_{b1}}{\varkappa^2} + \dfrac{1 + c_{b2}}{\sigma}$, $\tilde{S} = \left| \dfrac{\partial u}{\partial y} - \dfrac{\partial v}{\partial x} \right| + f_{\nu 2} \dfrac{\tilde{\nu}}{\varkappa^2 d^2}$, $f_{\nu 1} = \dfrac{\chi^3}{\chi^3 + c^3_{\nu 1}}$, $f_{\nu 2} = 1 - \dfrac{\chi}{1 + \chi f_{\nu 1}}$, $f_w = g \left(\dfrac{1 + c^6_{w3}}{g^6 + c^6_{w3}} \right)^{1/6}$, $\chi = \dfrac{\tilde{\nu}}{\nu}$, $r = \dfrac{\tilde{\nu}}{\tilde{S} \varkappa^2 d^2}$, $c_{t3} = 1.2$, $c_{t4} = 0.5$, $c_{w2} = 0.3$, $c_{w3} = 2$, $c_{\nu 1} = 7.1$, $c_{b1} = 0.1355$, $c_{b2} = 0.622$, $\varkappa = 0.41$, $\sigma = 2/3$.

The 'Trip-Less' (TL) approach [6] is used: firstly very high value of the S-A working variable is setted on inlet boundary and then once a separation zone is formed value of the S-A working variable on inlet boundary is greatly reduced. Thus, the boundary conditions for (8) take the following form:

$$\tilde{\nu}|_{\text{airfoil}} \equiv 0, \quad \left. \frac{\partial \tilde{\nu}}{\partial \mathbf{n}} \right|_{\text{outlet}} = 0, \quad \tilde{\nu}|_{\text{inlet}} = \tilde{\nu}_\infty(t) = \begin{cases} \nu, \ t \le t^*, \\ 0.001\nu, \ t > t^*. \end{cases} \tag{9}$$

3 MAIN IDEAS OF THE LS-STAG METHOD

The Cartesian mesh with cells $\Omega_{i,j} = (x_{i-1}, x_i) \times (y_{j-1}, y_j)$ is introduced in the rectangular computational domain Ω. It is denoted that $\Gamma_{i,j}$ is the face of $\Omega_{i,j}$ and $\mathbf{x}^c_{i,j} = (x^c_i, y^c_j)$ is the center of this cell. Unknown components $u_{i,j}$ and $v_{i,j}$ of velocity vector $\mathbf{v}$ are computed in the middle of fluid parts of the cell faces. These points are the centers of cells $\Omega^u_{i,j} = (x^c_i, x^c_{i+1}) \times (y_{j-1}, y_j)$ and $\Omega^v_{i,j} = (x_{i-1}, x_i) \times (y^c_j, y^c_{j+1})$ with faces $\Gamma^u_{i,j}$ and $\Gamma^v_{i,j}$ and areas M^x_{ij} and $M^y_{i,j}$ respectively. If $i = \overline{1, N}$, $j = \overline{1, M}$, the base mesh contains $E = N \cdot M$ cells, x-mesh contains $E_x = (N-1) \cdot M$ cells and y-mesh contains $E_y = N \cdot (M-1)$.

The level-set function $\varphi = \varphi(x, y)$ [3] is introduced for immersed boundary Γ^{ib} description [2]. The boundary Γ^{ib} is represented by a line segment on the cut-cell $\Omega_{i,j}$. Locations of this segment endpoints are defined by a linear interpolation of the variable $\varphi_{i,j} = \varphi(x_i, y_j)$. The cell-face fraction ratios $\vartheta^u_{i,j}$ and $\vartheta^v_{i,j}$ are introduced [2]. They take values in interval $[0, 1]$ and represent the fluid parts of the east and north faces of $\Gamma_{i,j}$ respectively. In 2D case, the cut-cells can be classified into trapezoidal, triangular and pentagonal cells. Examples of each type cut-cells are presented on fig. 1.

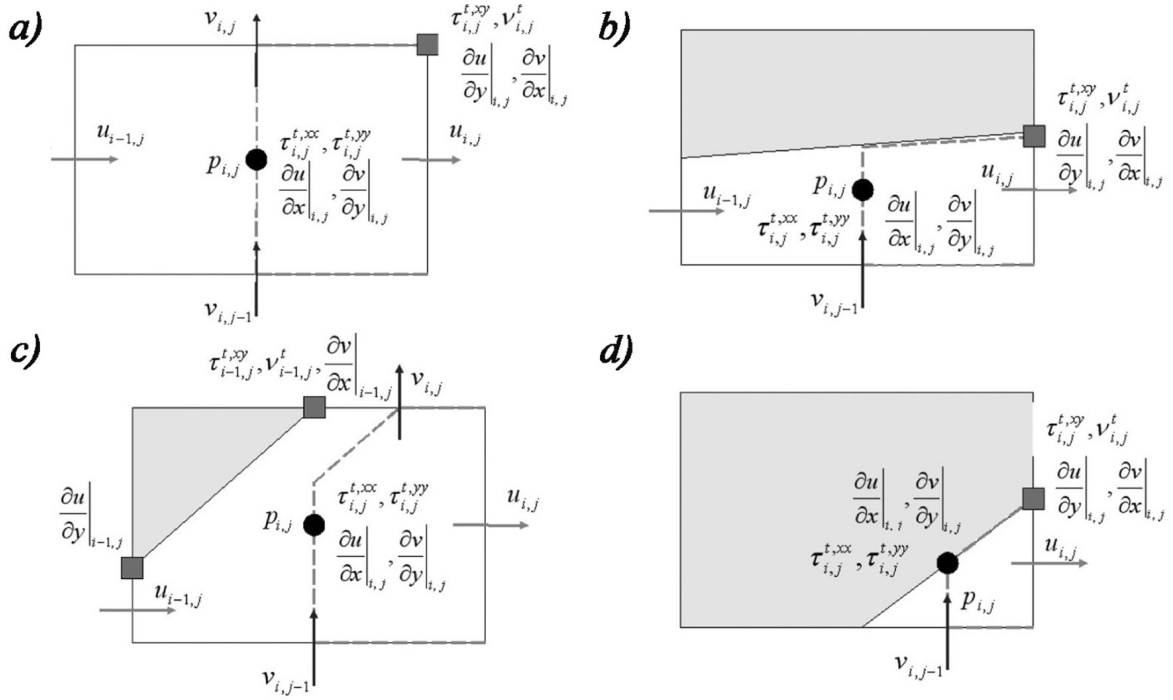

Figure 1: Location of the variables discretization points on the LS-STAG mesh: *(a)* Cartesian Fluid Cell; *(b)* North Trapezoidal Cell; *(c)* Northwest Pentagonal Cell; *(d)* Northwest Triangle Cell.

To preserve the five-point stencil structure of the MAC method we need to make distinction between the discretization of the normal and shear stresses (fig. 1). The normal stresses are sampled in the center of $\Omega_{i,j}$ cell while the shear stresses are sampled

in its corners. Normal and shear Reynolds stresses are sampled similarly. It is conveniently to sample the eddy viscosity and the S-A working variable at the same points as the shear stresses. Thus, in case of the LS-STAG method usage for RANS-based models we need the fourth mesh (xy-mesh with $E_{xy} = (N-1)\cdot(M-1)$ cells) with cells $\Omega^{xy}_{i,j} = (x^c_i, x^c_{i+1}) \times (y^c_j, y^c_{j+1})$. The faces of these cells are $\Gamma^{xy}_{i,j}$ and their areas are $M^{xy}_{i,j}$.

4 THE GENERAL FORM OF THE LS-STAG DISCRETIZATION FOR RANS EQUATIONS

According to the concept of the LS-STAG method equations (1) should be written in integral form for cell of the base mesh, cell of x-mesh and cell of y-mesh respectively:

$$\int\limits_{\Gamma_{i,j}} \mathbf{v}\cdot\mathbf{n}\, dS = 0, \tag{10}$$

$$\frac{d}{dt}\int\limits_{\Omega^u_{i,j}} u\, dV + \int\limits_{\Gamma^u_{i,j}} (\mathbf{v}\cdot\mathbf{n}) u\, dS + \int\limits_{\Gamma^u_{i,j}} p\mathbf{e_x}\cdot\mathbf{n}\, dS - \int\limits_{\Gamma^u_{i,j}} \nu\nabla u\cdot\mathbf{n}\, dS - \underline{\int\limits_{\Gamma^u_{i,j}} \tau^t_{xx}\mathbf{e_x}\cdot\mathbf{n}\, dS} - \underline{\underline{\int\limits_{\Gamma^u_{i,j}} \tau^t_{xy}\mathbf{e_y}\cdot\mathbf{n}\, dS}} = 0,$$

$$\frac{d}{dt}\int\limits_{\Omega^v_{i,j}} v\, dV + \int\limits_{\Gamma^v_{i,j}} (\mathbf{v}\cdot\mathbf{n}) v\, dS + \int\limits_{\Gamma^v_{i,j}} p\mathbf{e_y}\cdot\mathbf{n}\, dS - \int\limits_{\Gamma^v_{i,j}} \nu\nabla v\cdot\mathbf{n}\, dS - \underline{\int\limits_{\Gamma^v_{i,j}} \tau^t_{yy}\mathbf{e_y}\cdot\mathbf{n}\, dS} - \underline{\underline{\int\limits_{\Gamma^v_{i,j}} \tau^t_{xy}\mathbf{e_x}\cdot\mathbf{n}\, dS}} = 0.$$

Formally, the difference between the integral form of the RANS equations (10) and integral form of the Navier–Stokes equations, for which the LS-STAG discretization was constructed in [2], is only presence of the underlined terms.

The general form of the LS-STAG discretization for (10) can be written as the following:

$$D^x U_x + D^y U_y + \overline{U}^{ib} = 0, \tag{11}$$

$$\frac{d}{dt}(M^x U_x) + C^x U_x + G^x(P - \underline{T_{xx}}) - \underline{\underline{D^\tau_x T_{xy}}} - \nu K^x U_x + S^{ib,c}_x - \nu S^{ib,\nu}_x = 0,$$

$$\frac{d}{dt}(M^y U_y) + C^y U_y + G^y(P - \underline{T_{yy}}) - \underline{\underline{D^\tau_y T_{xy}}} - \nu K^y U_y + S^{ib,c}_y - \nu S^{ib,\nu}_y = 0.$$

Here $P\in\mathbb{R}^E$ is the discrete pressure, $U_x\in\mathbb{R}^{E_x}$ and $U_y\in\mathbb{R}^{E_y}$ are the discrete components of the velocity vector, $T_{xy}\in\mathbb{R}^{E_{xy}}$ is the discrete shear Reynolds stresses, $T_{xx}\in\mathbb{R}^E$ and $T_{yy}\in\mathbb{R}^E$ are the discrete normal Reynolds stresses; $S^{ib,c}_x\in\mathbb{R}^{E_x}$, $S^{ib,\nu}_x\in\mathbb{R}^{E_x}$, $S^{ib,c}_y\in\mathbb{R}^{E_y}$, $S^{ib,\nu}_y\in\mathbb{R}^{E_y}$ are source terms; $\overline{U}^{ib}\in\mathbb{R}^E$ is the mass flux; $D^x\in M(\mathbb{R})_{E\times E_x}$, $D^y\in M(\mathbb{R})_{E\times E_y}$, $D^\tau_x\in M(\mathbb{R})_{E_x\times E_{xy}}$, $D^\tau_y\in M(\mathbb{R})_{E_y\times E_{xy}}$ are the divergence discrete analogues; $K^x\in M(\mathbb{R})_{E_x\times E_x}$ and $K^y\in M(\mathbb{R})_{E_y\times E_y}$ represent the discretization of the diffusive terms; $C^x\in M(\mathbb{R})_{E_x\times E_x}$ and $C^y\in M(\mathbb{R})_{E_y\times E_y}$ represent the discretization of the convective terms; $G^x = -D^T_x$ and $G^y = -D^T_y$ are the gradient discrete analogues.

As in [2], matrices D^x and D^y have the following structure ($i = \overline{1,N}$, $j = \overline{1,M}$):

$$D^x_P(i,j)=\vartheta^u_{i,j}\Delta y_j,\ D^x_W(i,j)=-\vartheta^u_{i-1,j}\Delta y_j,\ D^y_P(i,j)=\vartheta^v_{i,j}\Delta x_i,\ D^y_S(i,j)=-\vartheta^v_{i,j-1}\Delta x_i. \quad (12)$$

We need to construct the LS-STAG discretization of terms with shear Reynolds stress underlined by two lines in (10), as they appear only in the RANS equations. Both for rectangular cells, and for all types of cut-cells the following unified formulae can be written down:

$$\int\limits_{\Gamma^u_{i,j}} \tau^t_{xy}\mathbf{e_y}\cdot\mathbf{n}\,dS \approx \frac{1}{2}(\vartheta^v_{i,j}\Delta x_i + \vartheta^v_{i+1,j}\Delta x_{i+1})\tau^t_x|_{i,j} - \frac{1}{2}(\vartheta^v_{i,j-1}\Delta x_i + \vartheta^v_{i+1,j-1}\Delta x_{i+1})\tau^t_{xy}|_{i,j-1}, \quad (13)$$

$$\int\limits_{\Gamma^v_{i,j}} \tau^t_{xy}\mathbf{e_x}\cdot\mathbf{n}\,dS \approx \frac{1}{2}(\vartheta^u_{i,j}\Delta y_j + \vartheta^u_{i,j+1}\Delta y_{j+1})\tau^t_{xy}|_{i,j} - \frac{1}{2}(\vartheta^u_{i-1,j}\Delta y_j + \vartheta^u_{i-1,j+1}\Delta y_{j+1})\tau^t_{xy}|_{i-1,j}.$$

Thus, matrices D^τ_x and D^τ_y in (11) can be defined as the following:

$$\begin{array}{l} i = \overline{1,N-1}: \left\{ \begin{array}{l} D^\tau_{x,P}(i,j) = (\vartheta^v_{i,j}\Delta x_i + \vartheta^v_{i+1,j}\Delta x_{i+1})/2,\ j = \overline{1,M-1}; \\ D^\tau_{x,S}(i,j) = -(\vartheta^v_{i,j-1}\Delta x_i + \vartheta^v_{i+1,j-1}\Delta x_{i+1})/2,\ j = \overline{2,M}; \end{array} \right. \\ j = \overline{1,M-1}: \left\{ \begin{array}{l} D^\tau_{y,P}(i,j) = (\vartheta^u_{i,j}\Delta y_j + \vartheta^u_{i,j+1}\Delta y_{j+1})/2,\ i = \overline{1,N-1}; \\ D^\tau_{y,W}(i,j) = -(\vartheta^u_{i-1,j}\Delta y_j + \vartheta^u_{i-1,j+1}\Delta y_{j+1})/2,\ i = \overline{2,N}. \end{array} \right. \end{array} \quad (14)$$

The time integration of the differential algebraic system (11) is performed with a semi-implicit Euler scheme. Predictor step leads to discrete analogues of the Helmholtz equation for velocities prediction $\widetilde{U}_x$, $\widetilde{U}_y$ at the time $t_{n+1} = (n+1)\Delta t$:

$$\frac{M^{n+1}_x\widetilde{U}_x - M^n_x U^n_x}{\Delta t} + C^n_x U^n_x + S^{ib,c,n}_x - D^{T,n}_x(P^n - \underline{T^n_{xx}}) - \underline{\underline{D^{\tau,n}_x T^n_{xy}}} - \nu K^{n+1}_x\widetilde{U}_x - \nu S^{ib,\nu,n+1}_x = 0, \quad (15)$$

$$\frac{M^{n+1}_y\widetilde{U}_y - M^n_y U^n_y}{\Delta t} + C^n_y U^n_y + S^{ib,c,n}_y - D^{T,n}_y(P^n - \underline{T^n_{yy}}) - \underline{\underline{D^{\tau,n}_y T^n_{xy}}} - \nu K^{n+1}_y\widetilde{U}_y - \nu S^{ib,\nu,n+1}_y = 0.$$

Here Δt is the constant time discretization step. Corrector step leads to the following discrete analogue of Poisson equation for $\Phi = \Delta t(P^{n+1} - P^n)$:

$$A^{n+1}\Phi = D^{n+1}_x\widetilde{U}_x + D^{n+1}_y\widetilde{U}_y + \overline{U}^{ib,n+1}, \quad (16)$$

$A = -D^x(M^x)^{-1}(D^x)^T - D^y(M^y)^{-1}(M^y)^T$, $A \in M(\mathbb{R})_{E\times E}$. Then flow variables at the time t_{n+1} are computed by the following formulae:

$$U^{n+1}_x = \widetilde{U}_x + (M^{n+1}_x)^{-1}D^{T,n+1}_x\Phi,\ U^{n+1}_y = \widetilde{U}_y + (M^{n+1}_y)^{-1}D^{T,n+1}_y\Phi,\ P^{n+1} = \frac{\Phi}{\Delta t} + P^n. \quad (17)$$

After this step in case of RANS equations, new values of Reynolds stresses T^{n+1}_{xx}, T^{n+1}_{yy}, T^{n+1}_{xy} are computed by solving the discrete analogues of the corresponding equations. It should be noted that linear systems are solved using the BiCGStab method [7] with the ILU- and multigrid [8] preconditioning. An original algorithm for the solver cost-coefficient estimation [9] is used for the optimal parameters choice for the multigrid preconditioner.

5 EXTENSION OF THE LS-STAG METHOD FOR THE SPALLART — ALLMARAS TURBULENCE MODEL

Since the eddy viscosity and shear Reynolds stresses sampling points are the same, according to (7) it is possible to write down:

$$\tau^t_{xy}|_{i,j} = \nu^t_{i,j}\left(\left.\frac{\partial u}{\partial y}\right|_{i,j} + \left.\frac{\partial v}{\partial x}\right|_{i,j}\right). \tag{18}$$

The eddy viscosity average on the cell $\Omega_{i,j}$ of the base mesh should be used for normal Reynolds stresses computing (6):

$$\tau^t_{xx}|_{i,j} = 2\overline{\nu^t}_{i,j}\left.\frac{\partial u}{\partial x}\right|_{i,j},\ \tau^t_{yy}|_{i,j} = 2\overline{\nu^t}_{i,j}\left.\frac{\partial v}{\partial y}\right|_{i,j},\ \overline{\nu^t}_{i,j} = \alpha_{i,j}(\nu^t_{i,j} + \nu^t_{i,j-1} + \nu^t_{i-1,j} + \nu^t_{i-1,j-1}), \tag{19}$$

$$\alpha_{i,j} = \begin{cases} 0, & \text{if } \Omega_{i,j} \text{ is a solid cell,} \\ 1/3, & \text{if } \Omega_{i,j} \text{ is a triangular cell,} \\ 1/4, & \text{otherwise.} \end{cases}$$

Moreover, the eddy viscosity reconstructing by S-A working variable (8) is performed in the obvious way, since ν^t, $\tilde{\nu}$ and $f_{\nu 1}$ are computed at the same points.

The transport equation (8) in integral form has the following form:

$$\frac{d}{dt}\int\limits_{\Omega^*}\tilde{\nu}\,dV + \int\limits_{\Gamma^*}(\mathbf{v}\cdot\mathbf{n})\tilde{\nu}\,dS = \int\limits_{\Omega^*}(P^\nu - D^\nu)\,dV + \frac{1}{\sigma}\int\limits_{\Gamma^*}[\nu+\tilde{\nu}]\nabla\tilde{\nu}\cdot\mathbf{n}\,dS + \frac{c_{b2}}{\sigma}\int\limits_{\Omega^*}(\nabla\tilde{\nu})^2\,dV. \tag{20}$$

It is obvious that $\int\limits_{\Omega^{xy}_{i,j}}(P^\nu - D^\nu)\,dV \cong M^{xy}_{i,j}(P^\nu_{i,j} - D^\nu_{i,j}) = M^{xy}_{i,j}S_{i,j}$ because production and destruction terms are sampled at the same points as the S-A working variable.

Convenience of $\tilde{\nu}$ discretization on the xy-mesh consists mainly in the fact that due to this $\partial\tilde{\nu}/\partial x$ and $\partial\tilde{\nu}/\partial y$ are sampled on the y-mesh and x-mesh respectively:

$$\left.\frac{\partial\tilde{\nu}}{\partial x}\right|_{i,j} = \frac{\tilde{\nu}_{i,j} - \tilde{\nu}_{i-1,j}}{\vartheta^v_{i,j}\Delta x_i}, \quad \left.\frac{\partial\tilde{\nu}}{\partial y}\right|_{i,j} = \frac{\tilde{\nu}_{i,j} - \tilde{\nu}_{i,j-1}}{\vartheta^u_{i,j}\Delta y_j}. \tag{21}$$

The discretization of the last term in (20) is the following:

$$\int\limits_{\Omega^{xy}_{i,j}}(\nabla\tilde{\nu})^2\,dV \cong (\beta_{i+1,j} + \beta_{i+1,j+1})\left(\left.\frac{\partial\tilde{\nu}}{\partial x}\right|_{i+1,j}\right)^2 + (\beta_{i,j} + \beta_{i,j+1})\left(\left.\frac{\partial\tilde{\nu}}{\partial x}\right|_{i,j}\right)^2 + \tag{22}$$

$$+(\beta_{i,j} + \beta_{i+1,j})\left(\left.\frac{\partial\tilde{\nu}}{\partial y}\right|_{i,j}\right)^2 + (\beta_{i,j+1} + \beta_{i+1,j+1})\left(\left.\frac{\partial\tilde{\nu}}{\partial y}\right|_{i,j+1}\right)^2 = S^G_{i,j}.$$

Here $\beta_{i,j} = \alpha_{i,j}V_{i,j}$, $V_{i,j}$ is the area of $\Omega_{i,j}$ cell.

And for the diffusive term in (20) we obtain

$$\int\limits_{\Gamma_{i,j}^{xy}} [\nu+\tilde{\nu}]\nabla\tilde{\nu}\cdot\mathbf{n}\,dS \cong \tag{23}$$

$$\cong \frac{1}{2}\left(\frac{\Delta y_j(\vartheta^u_{i,j}+\vartheta^u_{i+1,j})}{2}+\frac{\Delta y_{j+1}(\vartheta^u_{i,j+1}+\vartheta^u_{i+1,j+1})}{2}\right)\frac{\partial\tilde{\nu}}{\partial x}\bigg|_{i+1,j}\left(\nu+\frac{\tilde{\nu}_{i,j}+\tilde{\nu}_{i+1,j}}{2}\right)-$$

$$-\frac{1}{2}\left(\frac{\Delta y_j(\vartheta^u_{i,j}+\vartheta^u_{i-1,j})}{2}+\frac{\Delta y_{j+1}(\vartheta^u_{i,j+1}+\vartheta^u_{i-1,j+1})}{2}\right)\frac{\partial\tilde{\nu}}{\partial x}\bigg|_{i,j}\left(\nu+\frac{\tilde{\nu}_{i,j}+\tilde{\nu}_{i-1,j}}{2}\right)+$$

$$+\frac{1}{2}\left(\frac{\Delta x_i(\vartheta^v_{i,j}+\vartheta^v_{i,j+1})}{2}+\frac{\Delta x_{i+1}(\vartheta^v_{i+1,j}+\vartheta^v_{i+1,j+1})}{2}\right)\frac{\partial\tilde{\nu}}{\partial y}\bigg|_{i,j+1}\left(\nu+\frac{\tilde{\nu}_{i,j}+\tilde{\nu}_{i,j+1}}{2}\right)-$$

$$-\frac{1}{2}\left(\frac{\Delta x_i(\vartheta^v_{i,j}+\vartheta^v_{i,j-1})}{2}+\frac{\Delta x_{i+1}(\vartheta^v_{i+1,j}+\vartheta^v_{i+1,j-1})}{2}\right)\frac{\partial\tilde{\nu}}{\partial y}\bigg|_{i,j}\left(\nu+\frac{\tilde{\nu}_{i,j}+\tilde{\nu}_{i,j-1}}{2}\right).$$

Then $K^{xy}\in M(\mathbb{R})_{E_{xy}\times E_{xy}}$ and $S^{\nu}_{xy}\in\mathbb{R}^{E_{xy}}$ can be defined:

$$\int\limits_{\Gamma_{i,j}^{xy}} [\nu+\tilde{\nu}]\nabla\tilde{\nu}\cdot\mathbf{n}\,dS \cong K^{xy}_S(i,j)\tilde{\nu}_{i,j-1}+K^{xy}_W(i,j)\tilde{\nu}_{i-1,j}+K^{xy}_P(i,j)\tilde{\nu}_{i,j}+ \tag{24}$$

$$+K^{xy}_E(i,j)\tilde{\nu}_{i+1,j}+K^{xy}_N(i,j)\tilde{\nu}_{i,j+1}+S^{\nu}_{xy,\ i,j}.$$

Similarly, discretization for the convective term in (20) on the xy-mesh is obtained:

$$\int\limits_{\Gamma_{i,j}^{xy}} (\mathbf{v}\cdot\mathbf{n})\tilde{\nu}\,dS \cong \frac{[\bar{u}_{es}]_-+[\bar{u}_{en}]_-}{4}\cdot\tilde{\nu}_{i+1,j}-\frac{[\bar{u}_{ws}]_++[\bar{u}_{wn}]_+}{4}\cdot\tilde{\nu}_{i-1,j}+ \tag{25}$$

$$+\frac{([\bar{u}_{es}]_++[\bar{u}_{en}]_+)-([\bar{u}_{ws}]_-+[\bar{u}_{wn}]_-)+([\bar{v}_{nw}]_++[\bar{v}_{ne}]_+)-([\bar{v}_{sw}]_-+[\bar{v}_{se}]_-)}{4}\cdot\tilde{\nu}_{i,j}+$$

$$+\frac{[\bar{v}_{nw}]_-+[\bar{v}_{ne}]_-}{4}\cdot\tilde{\nu}_{i,j+1}-\frac{[\bar{v}_{sw}]_++[\bar{v}_{se}]_+}{4}\cdot\tilde{\nu}_{i,j-1},$$

$$\bar{u}_{es}=\bar{u}_{i,j}+\bar{u}_{i+1,j},\ \bar{u}_{en}=\bar{u}_{i,j+1}+\bar{u}_{i+1,j+1},\ \bar{u}_{ws}=\bar{u}_{i,j}+\bar{u}_{i-1,j},\ \bar{u}_{wn}=\bar{u}_{i,j+1}+\bar{u}_{i-1,j+1},$$

$$\bar{v}_{nw}=\bar{v}_{i,j}+\bar{v}_{i,j+1},\ \bar{v}_{ne}=\bar{v}_{i+1,j}+\bar{v}_{i+1,j+1},\ \bar{v}_{sw}=\bar{v}_{i,j}+\bar{v}_{i,j-1},\ \bar{v}_{se}=\bar{v}_{i+1,j}+\bar{v}_{i+1,j-1},$$

$$\bar{u}_{i,j}=\vartheta^u_{i,j}u_{i,j}\Delta y_j,\quad \bar{v}_{i,j}=\vartheta^v_{i,j}v_{i,j}\Delta x_i,\quad [c]_+=(c+|c|)/2,\quad [c]_-=(c-|c|)/2.$$

This leads to matrix $C^{xy}\in M(\mathbb{R})_{E_{xy}\times E_{xy}}$. Additionally, the $S^{c}_{xy}\in\mathbb{R}^{E_{xy}}$ contains a non-zero components, which correspond to the boundaries of the computational domain.

Thus, the following difference analogue of (20) is obtained:

$$\tilde{\nu}^{n+1}=(M^{xy,n+1})^{-1}\left[M^{xy,n}\{\tilde{\nu}^n+\Delta t\cdot S^n\}+\Delta t\left(\frac{K^{xy,n}\tilde{\nu}^n+S^{\nu,n}_{xy}+c_{b2}S^{G,n}}{\sigma}-C^{xy,n+1}\tilde{\nu}^n-S^{c,n}_{xy}\right)\right]. \tag{26}$$

6 NUMERICAL EXPERIMENTS

6.1 Flow past a fixed circular airfoil

The flow past circular airfoil was simulated using the developed modification of the LS-STAG method at the Reynolds numbers Re = 1000 (on non-uniform meshes 120×148 with $\Delta t = 5 \cdot 10^{-2}$ and 240×296 with $\Delta t = 10^{-3}$) and Re = 3900 (on non-uniform meshes 120×148 with $\Delta t = 10^{-3}$ and 240×296 with $\Delta t = 5 \cdot 10^{-4}$). These values of the Re were chosen because the experimental data [10] and results of other researchers [11, 12, 13] are known for them. The time averaged drag coefficient C_D and the Strouhal number St were computed. Computational results are shown in table 1. These results are in good agreement with experimental data for simulation on coarse meshes by using the proposed modification of the LS-STAG method.

Table 1: Comparison of C_D and St with established results from the literature.

Turbulence model	Number of cells	Re = 1000		Re = 3900	
		C_D	St	C_D	St
Experiment [10]		0.98	0.21	0.93	0.22
LES [11]	1 103 520	—	—	1.08	—
S-A, present study	17 760	1.12	0.26	0.86	0.18
S-A, present study	71 040	1.03	0.25	1.12	0.25
$k - \varepsilon$ [12]	46 304	1.00	0.15	1.00	0.15
Real $k - \varepsilon$ [12]	46 304	—	0.17	—	0.20
SST $k - \omega$ [12]	46 304	—	0.23	—	0.25
$k - \varepsilon$ [13], ANSYS	388 550	1.17	—	0.74	—
SST $k - \omega$ [13], ANSYS	388 550	0.99	—	0.62	—
LES [13], ANSYS	388 550	1.15	0.21	1.07	—

6.2 Circular airfoil wind resonance

Coupled aeroelastic problems appear when simulating autorotation and auto-oscillations phenomena, in particular, airfoil wind resonance. Such problems are complicated for numerical solution, since it is necessary to take into account interference between the flow and moving immersed body. In case of sufficiently massive body, coupled aeroelastic problems can be solved using step-by-step splitting numerical algorithm, firstly simulating flow around a body moving with known parameters and then computing the dynamics of the body with known hydrodynamic loads [14].

To simulate wind resonance phenomenon we have considered the motion of the circular airfoil with diameter D across the stream (with one degree of freedom). Airfoil's constrain assumed to be linear viscoelastic and its motion (4) is described by the following ordinary

differential equation:

$$m\ddot{y}_* + b\dot{y}_* + cy_* = F_y. \tag{27}$$

Here m is the airfoil's mass, b is the damping factor, c is the constraint's elasticity, F_y is lift force, y_* is the deviation from the equilibrium. The natural frequency of the system $\omega \approx \sqrt{c/m}$ (damping assumed to be small) can be set by varying of the coefficient c.

Number of computations have been performed on non-uniform grid 272×292 with time discretization step $\Delta t = 0.0001$ and the following dimensionless parameters: $\mathrm{Re} = 1000$, $V_\infty = 3.0$, $m = 39.15$, $b = 0.731$. The dimensionless natural frequency of the system is the following:

$$\mathrm{Sh}_\omega = \frac{\omega}{2\pi} \cdot \frac{D}{V_\infty} = 0.150 \ldots 0.280. \tag{28}$$

Computational results are in good agreement with the previous studies [15]. Maximum amplitude (fig. 2) is about $0.4D$ and it occures when the natural frequency of the system St_ω is close to the Strouhal number, calculated for a fixed airfoil $\mathrm{St} \approx 0.24$ [2].

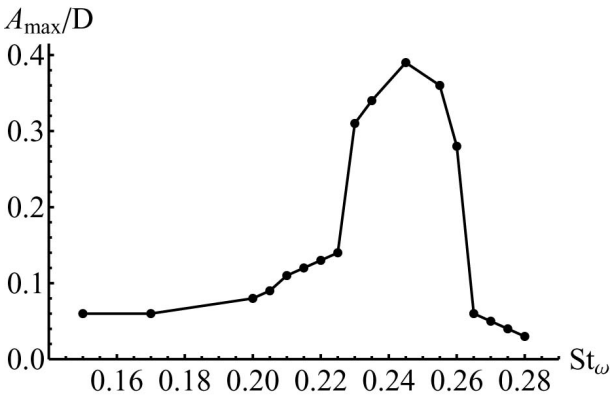

Figure 2: Maximum amplitude of the circular airfoil oscillations at $\mathrm{Re} = 1000$

7 CONCLUSIONS

- The key points of the LS-STAG method extension for RANS-based turbulence models are described. For the shear Reynolds stresses and for the eddy viscosity an additional mesh (xy-mesh) is introduced.

- The general approach to the construction of the LS-STAG discretization for differential equations of the EVM RANS models on the additional xy-mesh is shown on the example of the Spalarat — Allmaras model.

- A software package is developed for the numerical simulation of the bodies' motion in the viscous incompressible flow by using the LS-STAG method and its modifications.

- To validate this approach and the developed software package the flow past a circular airfoil at the Reynolds number values Re = 1000 and Re = 3900 was simulated. Computational results are in good agreement with established results from the literature.

- Simulation of a circular airfoil wind resonance phenomenon is considered. Computational results are in good qualitative agreement with the experimental data.

8 ACKNOWLEGEMENTS

The work was partially supported by Russian Federation President Grant for young scientists [proj. MK-3705.2014.8, MK-5357.2015.8].

REFERENCES

[1] Mittal, R. and Iaccarino, G. Immersed boundary methods. *Annu. Rev. Fluid Mech.* (2005) **37**:239–261.

[2] Cheny, Y. and Botella, O. The LS-STAG method: A new immersed boundary/level-set method for the computation of incompressible viscous flows in complex moving geometries with good conservation properties. *J. Comput. Phys.* (2010) **229**:1043–1076.

[3] Osher, S. and Fedkiw, R.P. *Level set methods and dynamic implicit surfaces.* Springer, (2003).

[4] Spalart, P.R. Strategies for turbulence modelling and simulations. *Int. J. Heat and Fluid Flow.* (2000). **21**: 252–263.

[5] Spalart, P.R. and Allmaras, S.R. A one-equation turbulence model for aerodynamic flows. *Recherche Aerospatiale.* (1994). **1**: 5–21.

[6] Shur, M., Spalart, P., Strelets, M. and Travin, A. Navier-Stokes simulation of shedding turbulent flow past a circular cylinder and a cylinder with backward splitter plate. *Comp. Fluid Dyn.* (1996). **96**: 676–682.

[7] Van der Vorst, H.A. Bi-CGSTAB: a fast and smoothly converging variant of Bi-CG for solution of non-symmetric linear systems. *SIAM J. Sci. Stat. Comp.* (1992). **2**:631–644.

[8] Wesseling, P. *An introduction to multigrid methods.* John Willey & Sons Ltd., (1991).

[9] Marchevsky, I.K. and Puzikova, V.V. OpenFOAM iterative methods efficiency analysis for linear systems solving. *Proceedings of the Institute for System Programming of RAS.* (2013) **24**:71–86. [in Russian]

[10] Zdravkovich, M.M. *Flow around circular cylinders.* Oxford University Press, (1997).

[11] Breuer, M. Large Eddy Simulation of the subcritical flow past a circular cylinder: numerical and modelling aspects. *Int. J. Numer. Meth. Fluids.* (1998). **28**: 1281–1302.

[12] Rahman, M.M., Karim, M.M. and Alim, M.A. Numerical investigation of unsteady flow past a circular cylinder using 2-D finite volume method. *J. Naval Arch. and Marine Eng.* (2007). **4**: 27–42.

[13] Patel, Y. *Numerical Investigation of flow past a circular cylinder and in a staggered tube bundle using various turbulence models. Master's thesis.* Lappeenranta University of Technology, (2010).

[14] Puzikova, V.V. and Marchevsky, I.K. Application of the LS-STAG immersed boundary method for numerical simulation in coupled aeroelastic problems. *Proceedings of 11th World Congress on Computational Mechanics (WCCM XI), 5th European Conference on Computational Mechanics (ECCM V), 6th European Conference on Computational Fluid Dynamics (ECFD VI).* (20–26 July 2014) :1995–2006.

[15] Klamo, J.T., Leonard, A. and Roshko, A. On the maximum amplitude for a freely vibrating cylinder in cross flow. *J. of Fluids and Struct.* (2005) **21**:429–434.